Theor Chem Acc (2012) 131:1177
DOI 10.1007/s00214-012-1177-z

REGULAR ARTICLE

Thermal and environmental effects on Oligothiophene low-energy singlet electronic excitations in dilute solution: a theoretical and experimental study

Massimiliano Aschi · Andrea Amadei · Andrea Pellegrino · Nicola Perin · Riccardo Po'

Received: 20 August 2011 / Accepted: 19 October 2011 / Published online: 2 March 2012

Abstract The absorption spectra in dilute dichloromethane solution at 300 K of four Oligotiophenes (OT), namely 2,2′:5′,2″-Terthiophene, 2,2′:5′,2″:5″,2‴-Quaterthiophene, 4,4‴-Didodecyl-2,2′:5′,2″:5″,2‴-quaterthiophene and 5,5‴′′-Dihexyl-2,2′:5′,2″:5″,2‴:5‴,2⁗:5⁗,2′′′′′-sexithiophene, have been studied both experimentally and theoretically by using a combination of molecular dynamics simulations, time-dependent density functional theory (TD-DFT) and perturbed matrix method calculations. A deep analysis of the theoretical results, affected by a systematic although not dramatic underestimation of the absorption maxima due to the well-documented TD-DFT limitations, clearly indicates that both the environmental (solvent) and thermal effects significantly alter the Oligotiophenes photophysical properties mainly because of the wide repertoire of the S_0–S_1 energy gaps and electronic densities experienced in solution by the different conformers actually populated. In particular, all the investigated OT display a very high flexibility resulting in a very high repertoire of sampled conformations. The comparison of the calculated and experimental lineshape of the S_0–S_1 electronic transition has clearly indicated that for a correct modeling of OT spectral features, the lack of an exhaustive sampling of semiclassical configurational space of the overall system, i.e., solute in interaction with the solvent, might result in an incomplete picture even in the presence of well-documented important aspects such as reliable definition of excited electronic states and the inclusion of quantum vibronic effects.

Keywords Oligothiophenes excited states modeling · Solar cell · Molecular dynamics · Quantum chemistry

Dedicated to Professor Vincenzo Barone and published as part of the special collection of articles celebrating his 60th birthday.

Electronic supplementary material The online version of this article (doi:10.1007/s00214-012-1177-z) contains supplementary material, which is available to authorized users.

M. Aschi (✉)
Dipartimento di Chimica, Ingegneria Chimica e Materiali Universita' di l'Aquila, Via Vetoio, 67100 Coppito I, l'Aquila, Italy
e-mail: aschi@caspur.it

A. Amadei
Dipartimento di Scienze e Tecnologie Chimiche, Universita' di Roma 'Tor Vergata', Via della Ricerca Scientifica, 00100 Rome, Italy

A. Pellegrino · N. Perin · R. Po'
Solar Energy Research Center for Non-Conventional Energies Istituto ENI Donegani Eni S.p.A, Via Giacomo Fauser 4, 28100 Novara, Italy

1 Introduction

Oligothiophenes (OT) are conjugated polycyclic thiophene oligomers extensively used in organic electronics [1] as light-emitting diodes [2] and solar cells [3] which have attracted, in the last years, a huge amount of experimental and theoretical work [4]. One of the most investigated aspects, considered to be fundamental for characterizing the photophysics of OT, is the full characterization of the low-lying singlet and triplet excited states involved in many photochemical processes, including electron transfer, taking place upon low-energy OT electronic excitations. Many studies have addressed the actual localization of the vertical and adiabatic singlet excited electronic states, the relative position of the first singlet excited state S_1 and the first triplet state T_1 [5–7], their dependency with respect the length of the OT chain [8–10], and the energetics and dynamics related to

the intra and intermolecular electron transfer upon excitation [11, 12].

Theoretical studies have also revealed that electronic-correlation, multi-reference wave-function, and multi-excitation character seem to be important ingredients to correctly reproduce OT electronic excitations [7, 13–18].

Accurate, and more recent, investigations carried out with different combinations of experimental and theoretical approaches have also revealed that a full understanding of OT spectral bandshapes requires a proper exploration of vibronic coupling [10, 19, 20].

As a matter of fact, OT species typically display, at low temperature, absorption spectra characterized by mirror symmetry.

However, temperature increase has been shown to produce spectral broadening [10] clearly indicating that thermal excitations of torsional modes producing different OT conformations [21–25] in interaction with the solvent [20, 26, 27] play a very important role in OT photophysics whose modeling should also take into account these effects.

As a consequence, several studies have recently proposed advanced theoretical modeling of OT spectral features including both vibronic coupling, torsional modes excitations and solvent effects [10, 19, 20].

However, the same studies [19, 20] have also clearly stated that OT have to be considered as soft materials hence plausibly characterized by a rather complicated conformational repertoire at relatively high temperature and in the presence of solvent inhomogeneity. In this respect, an unbiased and exhaustive sampling of the OT-solvent semiclassical conformational space—carried out with molecular dynamics (MD) simulations—associated with a proper treatment of the quantum degrees of freedom might greatly help in improving our understanding of the photophysics of these systems.

In line with our ongoing interest in the theoretical–computational modeling of electronic properties of molecular systems in solution, in the present investigation, we attempt to shed some light on the low-lying OT singlet excited states in solution in thermal conditions, i.e., explicitly taking into account thermal effects both on the OT conformational repertoire and on the solvent fluctuations.

In particular, we have considered the absorption spectra of four species in dilute CH_2Cl_2 solution at 300 K, namely 2,2′:5′,2″-Terthiophene (TT), 2,2′:5′,2″:5″,2‴-Quaterthiophene (QT), 4,4‴-Didodecyl-2,2′:5′,2″:5″,2‴-quaterthiophene (DQT), and 5,5⁗-Dihexyl-2,2′:5′,2″:5″,2‴:5‴, 2⁗:5⁗,2⁗⁗-sexithiophene (DET), schematically reported in Fig. 1. The experimental spectra of the above species have been compared with the corresponding spectra calculated in the same conditions utilizing a theoretical–computational scheme, based on MD simulations, Quantum-Chemical (QM) calculations, and the Perturbed Matrix Method (PMM) [28], extensively utilized in our laboratory in the last years for calculating the photophysical equilibrium properties, e.g., UV absorption spectrum, of molecules in solution [29–31].

Such a methodology, which might be considered somewhat complementary to more popular QM/MM approaches [32, 33] has been usually applied, so far, for characterizing the perturbed quantum states of rigid or semi-rigid molecules in solution. However, its extension to very flexible species such as OT [21] is relatively straightforward and, in the present investigation, its systematic implementation is presented for the first time. We wish to further remark that our goal in this work is not to provide an exact reproduction of OT low-lying singlet excited states in solution. In fact, the already cited effects such as multireference character of the wavefunction as well as inclusion of vibronic coupling [10, 19, 20], although already incorporated in our theoretical–computational setup [34], have been disregarded in the present investigation whose main aim is to specifically enucleate the effects of the solute and solvent conformational fluctuations onto the vertical low-lying singlet electronic excitations of solvated OT. Hence, well aware of its limitations for describing low-energy electronic excitations in OT [6, 15] and, more in general in π-conjugated species [35], Time-Dependent Density Functional Theory (TD-DFT) [36] has been adopted for characterizing OT unperturbed singlet electronic states. As a matter of fact, TD-DFT provides, at the moment, a very good compromise between costs and benefits when a huge number of geometries must be considered, as in the present case. In the first part of the study, the theoretical–computational method—hereafter concisely termed as PMM-MD—and the experimental setup are described in detail. Then, after a brief outline of the theoretical aspects of the work part, the experimental and computational results are presented and commented.

2 Theoretical and experimental methods

PMM-MD approach, similarly to many of the QM-MM methods [37], is based on the determination of the quantum states of a portion of a complex system (hereafter termed as Quantum Centre, QC), in interaction with the environment, e.g., the solvent molecules. The main differences with the other commonly employed approaches might be essentially summarized in two points:

- PMM-MD main goal is to maintain as much as possible, at a proper level of description, *both* the explicit definition of QC quantum degrees of freedom in interaction with the environment *and* an exhaustive

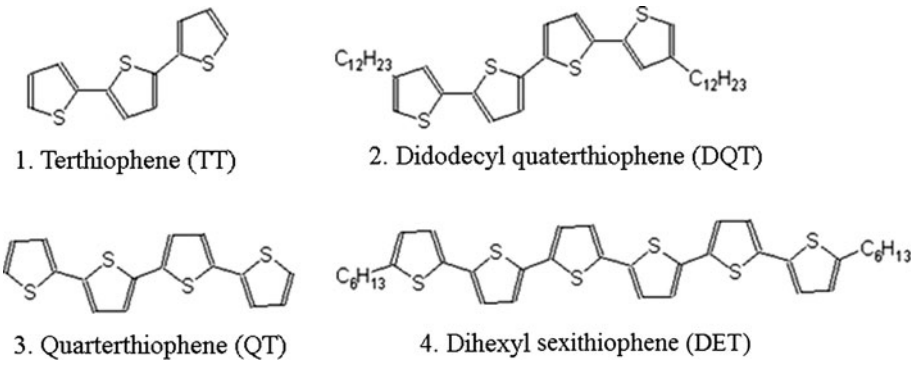

Fig. 1 Schematic representation of the species investigates in the present study

and significant sampling of the semiclassical phase-space of the overall system;

- differently from many of the commonly employed QM/MM methods, PMM-MD is based on a homogenous definition of the configurational space of the *overall* system, i.e., both the solute and the solvent are simulated according to classical MD making use of the *same* Hamiltonian. Subsequently, the configurations sampled by the overall system along MD simulation are utilized a posteriori to applying the PMM procedure for the evaluation of the QC ground to excited quantum (e.g., electronic) states interacting with the rest of the simulation box acting as a classical (e.g., electrostatic) perturbation. In the next three paragraphs, details of PMM, MD simulations, and the Quantum-Chemical (QM) calculations are reported.

2.1 Perturbed matrix method

The determination of the perturbed quantum (electronic) properties of the QC interacting with a classical perturbation along the MD simulation is achieved by defining, in matrix terms, a perturbed Hamiltonian (electronic) operator constructed on the basis set provided by the unperturbed (i.e., evaluated in vacuum) Born–Oppenheimer QC geometry, assumed for the moment to be characterized by a rigid covalent framework.

Hence, indicating with $\mathbf{r}_n$ the QC coordinates and with $\mathbf{x}(t)$ the atomic coordinates of the perturbing environment at a generic MD frame, we can write the perturbed electronic Hamiltonian matrix as

$$\tilde{H}[\mathbf{r}_n, \mathbf{x}(t)] = \tilde{H}^o(\mathbf{r}_n) + q_T V[\mathbf{r}_{\text{com}}, \mathbf{x}(t)] + \tilde{Z}_1[\mathbf{E}(\mathbf{r}_{\text{com}}, \mathbf{x}(t))] + \tilde{Z}_2\left[\tilde{\Theta}(\mathbf{r}_{\text{com}}, \mathbf{x}(t))\right] + \Delta\varsigma\tilde{I} \quad (1)$$

where $\tilde{H}^o(\mathbf{r}_n)$ is the unperturbed (gas-phase) electronic Hamiltonian calculated for the selected QC geometry (see Sect. 2.3), q_T is the QC total charge, $V[\mathbf{r}_{\text{com}}, \mathbf{x}(t)]$ and $\mathbf{E}$ are the electrostatic potential and electrostatic field exerted by perturbing molecules present in the simulation box at their instantaneous $\mathbf{x}(t)$ configuration and acting at the QC centre of mass ($\mathbf{r}_{\text{com}}$), and $\tilde{I}$is the identity matrix. The terms $\tilde{Z}_1[\mathbf{E}(\mathbf{r}_{\text{com}}, \mathbf{x}(t))]$ and $\tilde{Z}_2\left[\tilde{\Theta}(\mathbf{r}_{\text{com}}, \mathbf{x}(t))\right]$ are the perturbed Hamiltonian matrices whose generic l, l' elements are defined as:

$$\left[\tilde{Z}_1\right]_{l,l'} = -\mathbf{E} \cdot \left\langle \Phi_l^o \middle| \hat{\mu} \middle| \Phi_{l'}^o \right\rangle \quad (2)$$

and

$$\left[\tilde{Z}_2\right]_{l,l'} = \frac{1}{2} Tr[\tilde{\Theta}\tilde{Q}_{l,l'}] \quad (3)$$

where $\Theta_{k,k'} = \left(\frac{\partial E_k}{\partial r_{k'}}\right)_{\mathbf{r}=\mathbf{r}_{\text{com}}}$ is the electric field gradient evaluated at QC centre of mass and $\tilde{Q}_{l,l'}$ is the unperturbed l, l' transition quadrupole matrix, and $\Delta\varsigma$ is scalar term which approximates the perturbation due to all higher-order terms to simple short-range potential [28].

Note that in the case of dipolar approximation, i.e., first order, Eq. 1 can be rewritten as

$$\tilde{H}[\mathbf{r}_n, \mathbf{x}(t)] = \tilde{H}^o(\mathbf{r}_n) + q_T V[\mathbf{r}_{\text{com}}, \mathbf{x}(t)] + \tilde{Z}_1[\mathbf{E}(\mathbf{r}_{\text{com}}, \mathbf{x}(t))] + \Delta\varsigma'\tilde{I} \quad (4)$$

with the term (3), approximated in this case as a scalar term, merged together with $\Delta\varsigma$ into the same scalar term, $\Delta\varsigma'$. Both the transition dipole and transition quadrupole in (2) and (3) are derived by using the Φ_1^0 unperturbed electronic Hamiltonian eigenfunctions evaluated only once in correspondence of the QC (rigid) geometry. Diagonalization of the perturbed electronic Hamiltonian (Eq. 1 or 4) at each MD frame produces a trajectory of perturbed eigenvalues and eigenvectors ($\mathbf{c}_i$) of QC which can be used, in the present work, to evaluate at each configuration of the perturbing environment the perturbed excitation energies (i.e., the difference between the ith eigenvalue and the lowest eigenvalue of operator 1) and transition dipoles, $\boldsymbol{\mu}_{i,j}$, to be used for calculating the absorption spectra intensities [30], according to Eq. 5

$$\boldsymbol{\mu}_{i,j} = \mathbf{c}_\mathbf{i}^{*\mathbf{T}} \tilde{\Lambda}_x^0 \mathbf{c}_\mathbf{j} \mathbf{i} + \mathbf{c}_\mathbf{i}^{*\mathbf{T}} \tilde{\Lambda}_y^0 \mathbf{c}_\mathbf{j} \mathbf{j} + \mathbf{c}_\mathbf{i}^{*\mathbf{T}} \tilde{\Lambda}_z^0 \mathbf{c}_\mathbf{j} \mathbf{k} \quad (5)$$

where

$$[\tilde{\Lambda}_k^0]_{l,l'} = \langle \Phi_l^0 | \hat{\mu}_k | \Phi_{l'}^0 \rangle \quad (6)$$

The above PMM-MD procedure might be concisely described using the chart in Scheme 1 for a rigid QC.

These considerations are valid when the QC does not undergo conformational transitions, i.e., for a rigid covalent framework. Hence, it should be modified when, for the QC, several conformational states come out from MD simulation. In this case, we need to derive a set of unperturbed electronic Hamiltonian states ($\Phi_{l'}^{0-j}$) for each of the *j*th sampled conformation. Consequently, the PMM scheme modifies according to the Scheme 2.

The only additional problem, in this second case with respect to the rigid QC case, derives from the difficulty associated with the definition of the QC conformational transitions which becomes a relatively complicated task in the presence of more than one or two QC internal coordinates. This has been overcome using Essential Dynamics as described in the next paragraph dedicated to MD simulations details.

2.2 Molecular dynamics simulations and essential dynamics analysis

As already remarked, the overall system configurations are sampled by using a MD simulation with a properly selected (at a properly sophisticated level of theory) force field. The solute, i.e., in the case described in this paper each of the species 1–4 in Fig. 1, is put at the center of a rectangular box filled with dichloromethane (CH_2Cl_2) at the typical density of .786 g/ml at 300 K and 1.0 bar and simulated for

Scheme 1 Approximate flow chart for PMM application in the case of QC rigid geometry

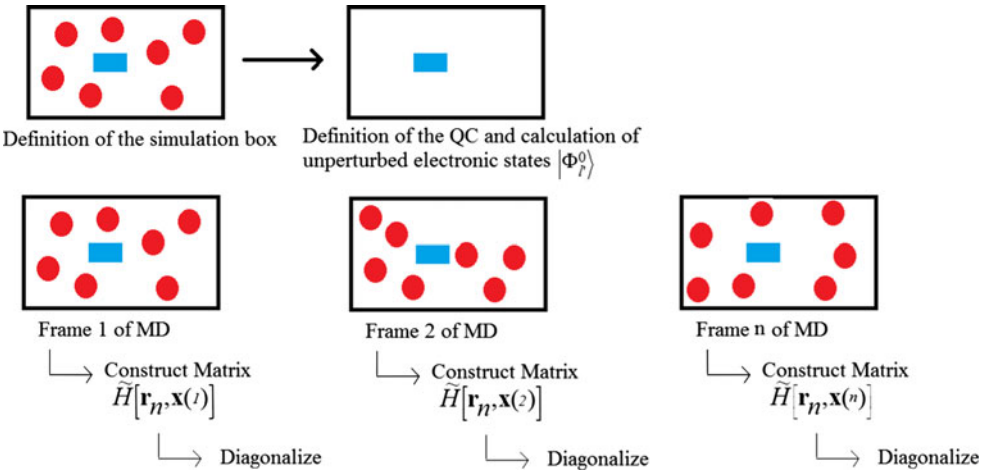

Scheme 2 Approximate flow chart for PMM application in the case of QC geometry transition. Note that the *blue square* and *triangle* correspond to different QC geometries

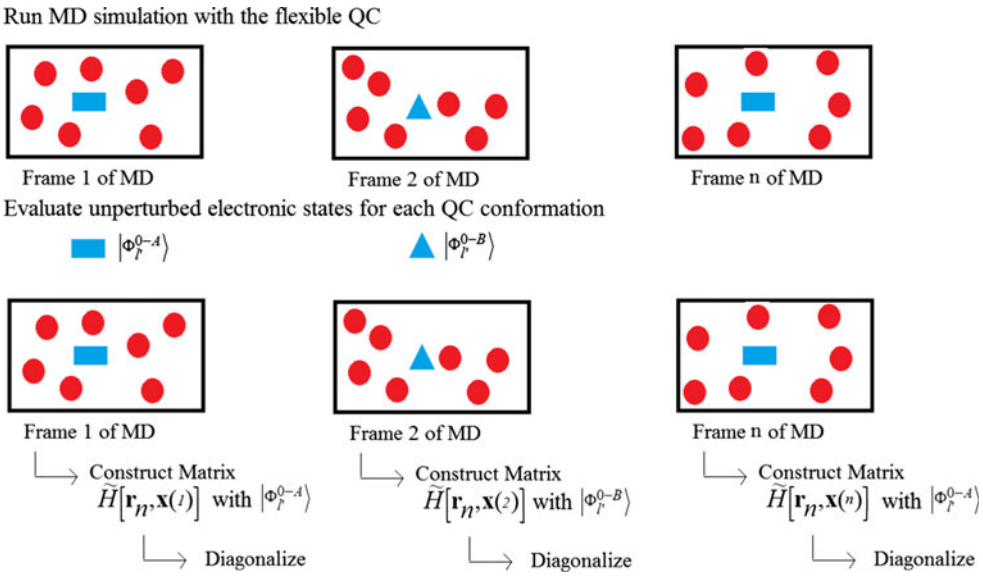

40 ns. For the species 1–4, we have adopted the force field recently developed by one of us [38]. For CH_2Cl_2, we used a force field adapted from opls-AA force field [39]. The following protocol was used for all the simulations: an energy minimization was first carried out and, after a solvent relaxation, the system was gradually heated from 50 to 300 K using short (typically 200.0 ps) MD simulations; the trajectories were then propagated up to 40 ns in a NVT ensemble using an integration step of 2 fs removing the solute roto-translation motions [40] (note that in the case of DQT and DET, only the OT moiety was used for the roto-translational fitting, see below); temperature was kept constant at 300 K by the Berendsen thermostat [41] with the τ equal to the time-step used for the integration algorithm. All bond lengths were constrained using LINCS algorithm [42]. Long-range electrostatics were computed by the Particle Mesh Ewald method [43] with 34 wave vectors in each dimension and a fourth-order cubic interpolation. Gromacs package [44] was used for all the simulations.

Essential Dynamics (ED) [45] was used for analyzing OT conformational transition. Briefly: using the equilibrated MD trajectory, the all-atoms OT covariance matrix was constructed and diagonalized. Such a transformation produces a set of eigenvectors which represent the directions along which OT fluctuates. Eigenvectors showing large eigenvalues define the space (essential space) in which the actual conformational transitions take place and are used for identifying the most stable (most sampled) conformations. In correspondence of these structures, unperturbed QM calculations are carried out as described in detail in the next Sect. 2.3.

2.3 Quantum-chemical calculations

On each of the *j*th conformation previously extracted from the essential space, we first carried out a geometrical relaxation of the quantum internal degrees of freedom (all bond lengths and angles) by keeping fixed all the dihedral angles using the B3LYP [46, 47] hybrid functional in conjunction to the 6–31 + G(d, p). These locally minimized structures were then used to obtain the ground and the first eight vertical excited states taken as basis set ($\Phi_{l'}^{0-j}$, $l' = 0, 1,\ldots,8$ in Scheme 2) utilizing TD-DFT calculations with the same functional and basis set. For these calculations, we used the Gaussian03 program [48].

2.4 Experimental setup

2,2′:5′,2″-Terthiophene (TT), 2,2′:5′,2″:5″,2‴-Quaterthiophene (QT), and 5,5‴″-Dihexyl-2,2′:5′,2″:5″,2‴:5‴,2⁗:5⁗,2⁗′:5⁗′,2⁗′-sexithiophene (DET) were purchased from Sigma-Aldrich Co., and used without purification. 4,4‴-Didodecyl-2,2′:5′,2″:5″,2‴-quaterthiophene (DQT) was prepared by Stille coupling of 2-tributylstannyl-4-dodecylthiophene and 2,2′-bithiophene-5,5′-dibromide and purified by column chromatography.

UV–Vis absorption spectra were recorded at room temperature with a Lambda 950 spectrophotometer (Perkin-Elmer Inc. Waltham, MA, USA). Samples in solution were prepared by dissolving the products in $CHCl_3$ (TT, QT, DQT, or DET) or CH_2Cl_2 (TT, QT, or DQT) solutions in cell with 10 mm optical path length and optical density of typically .5 at max. absorption in the visible region of spectrum.

3 Results

3.1 Experimental UV–Vis absorption spectra

The experimental UV–Visible spectra are reported in Fig. 2. All compounds present a band with maximum at 253 nm (only HST band is slightly red shifted). The main absorption band instead is red shifted with increase in π-conjugation of molecules. In particular, the maximum of absorption is centered at 355 nm for TT, 393 nm for QT, 398 nm for DQT, and 415 nm for DET. Note that DET was analyzed in $CHCl_3$ due to solubility problem anyway an experimental verification confirmed that for TT, QT, DQT the spectra in $CHCl_3$ and the spectra in CH_2Cl_2 are substantially the same.

Increasing the number of thiophene rings, the π-conjugation is enhanced and the maximum of absorption shifts to red. With the same number of thiophene rings, the alkyl side chains have influence on the maximum absorption band position; in fact, DQT is slightly red shifted compared

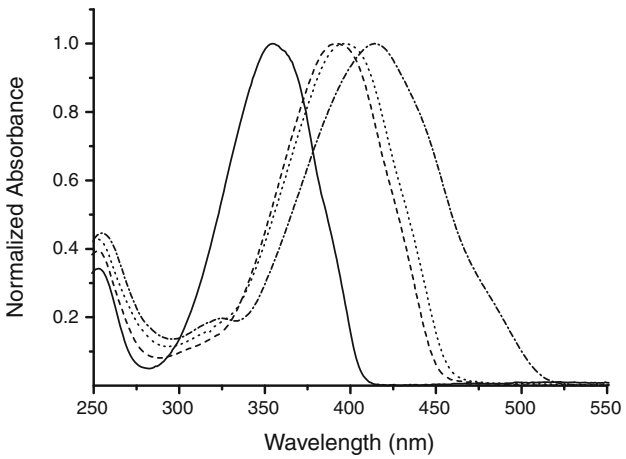

Fig. 2 UV–Visible absorption spectra of TT (*solid curve*), QT (*dash curve*), DQT (*dot curve*), and DET (*dash-dot curve*). All spectra are normalized at maximum of absorption and were recorded in CH_2Cl_2 solutions except DET that were recorded in $CHCl_3$ solutions

with QT due to inductive effect of alkyl side chains. In DET UV–Vis absorption spectrum, the shoulder on the red side might be due to some impurities, as confirmed by ^{1}H-NMR and mass spectra.

3.2 Extraction of the relevant conformations of OT moieties from MD simulation

For theoretically modeling the above spectra in this work, we assume that the electronic transitions we are looking at, i.e., essentially the S_0–S_1 and S_0–S_2 ones, essentially involve only the OT moieties in all the investigated species in Fig. 1. This approximation has been repeatedly shown, by the analysis of the molecular orbitals predominantly involved in low-lying valence excited excitations, to be acceptable in molecules similar of the ones addressed in this study [49]. It follows that in DQT and DET, the alkyl side chains have been assumed not to directly contribute to the electronic spectrum but their role is only relevant for the MD conformational sampling.

In the first part of this section, we analyze the OT moieties conformations sampled along the MD simulations to be used in the following PMM analysis.

In Fig. 3, we report the root mean square fluctuation (RMSF) of the four investigated systems in order to compare the internal mobility of the four species.

From Fig. 3, it is evident that, when present, alkyl side chains undergo a relatively large fluctuation and that all the systems are characterized by a rather high internal flexibility of the OT only slightly increasing with the dimension of the system. This means that all the species are expected to show a not negligible repertoire of OT conformations which should be in principle taken into account, with their own statistical weight, to construct the overall observed spectrum. A further aspect emerging from Fig. 3, which will turn out to be important for subsequent analyses, is the strong similarity between the RMSFs of OT moieties in QT and DQT systems.

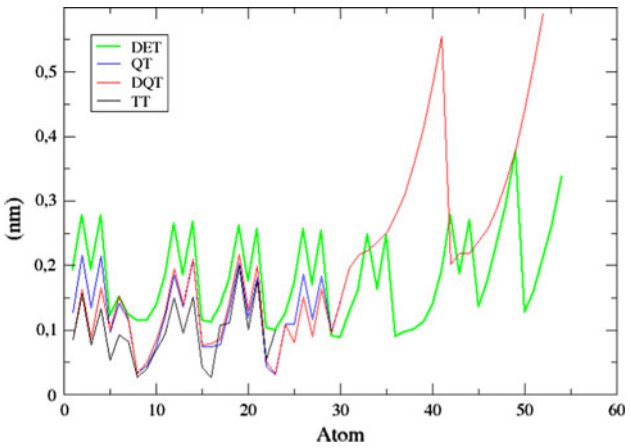

Fig. 3 Root mean square fluctuation for TT (*black*), QT (*blue*), DQT (*red*), and DET (*green*). Atoms starting from 31 for DQT and starting from 45 for DET correspond to alkyl side chains

The significant OT conformations sampled along the simulation have been extracted using ED as follows. First of all, it is important to underline that the construction and the diagonalization of the OT covariance matrix has produced for all the species a very steep spectrum of the eigenvalues indicating that the first and second eigenvector, accounting for almost the 70% of the overall fluctuation, would properly be used as the essential space for a correct conformational analysis.

Hence, the first step toward the extraction of OT geometries is represented by the projection of the trajectory onto such an essential space (i.e., essential plane, EP) producing differently populated portions (spots), hereafter termed as basins. An example of these basins is reported in Fig. 4a as a result of the ED analysis for TT species. Moreover, assuming the trajectory at the equilibrium, it is also possible to derive the relative stability, i.e., the relative

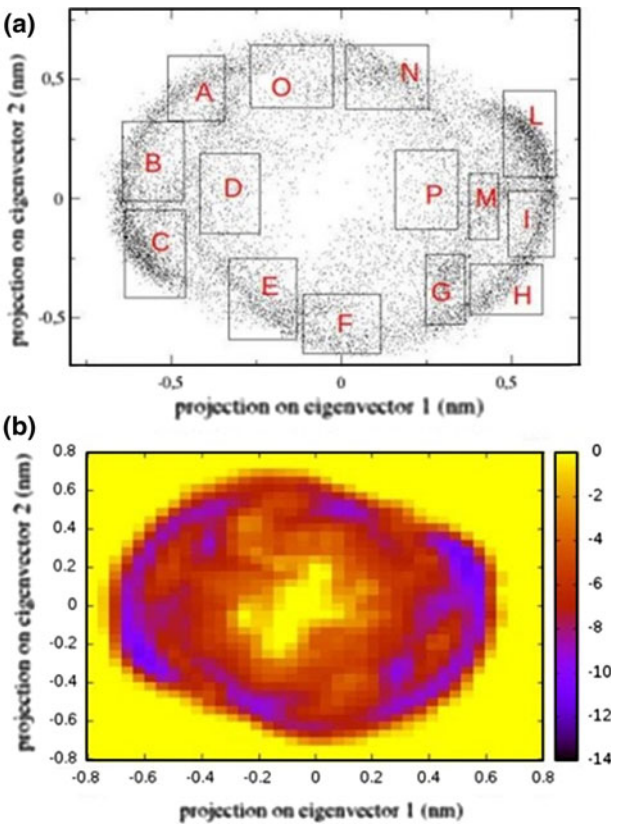

Fig. 4 **a** Identification of the conformational basins (*A*–*P*) on the TT essential plane and **b** corresponding 300 K Helmholtz free energy (kJ/mol) landscape from Eq. 7. Conformational basins are indicated with *red letters* and the representative structures are reported in the Supplementary Information *yellow* regions correspond to not sampled regions of the essential plane

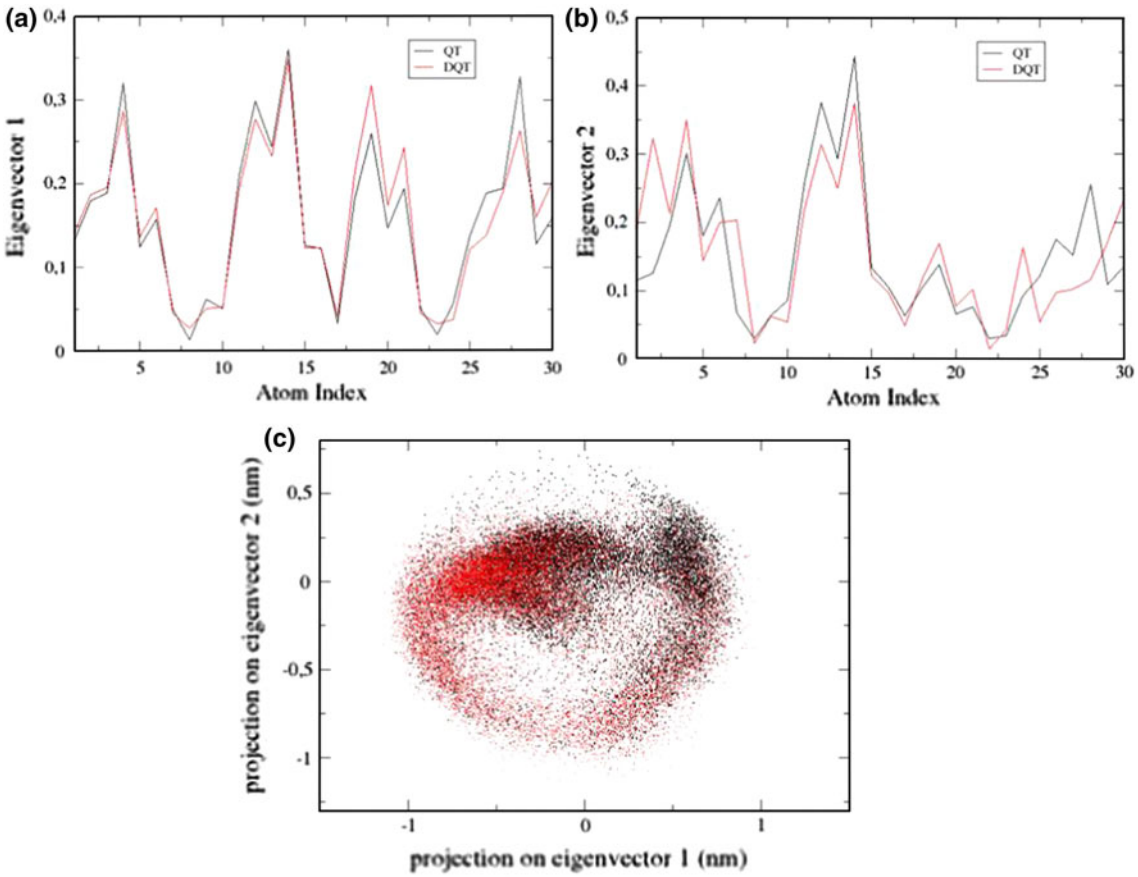

Fig. 5 Atom component of the first (**a**) and second (**b**) eigenvector from diagonalization of OT all-atom covariance matrix from MD simulation of QT (*black line*) and DQT (*red line*) in solution. **c** Projection of the QT (*black dots*) and DQT (*red dots*) trajectories on the corresponding essential plane

300 K Helmholtz free energy, for each OT basin using the standard formula

$$\Delta A_{i-ref} = A_i - A_{\text{ref}} = -\text{RTln}\frac{P_i}{P_{ref}} \quad (7)$$

where P_i and P_{ref} are the probability of finding the projected trajectory onto the basin *i* and *ref*, respectively. Note that the *ref* basin is the one showing the largest probability, in the case of TT the basin L. The resulting free energy landscape reported in Fig. 4b for TT indicates that all the basins lie within a free energy interval not exceeding 10 kJ/mol.

In correspondence of each basin, we then extract the OT conformations. This is obviously an approximation as a single geometrical conformation would strictly correspond to a single point on EP. However, as far as all the points (corresponding to different OT conformations) falling within a single basin display, as in the present case, geometrical deviations well below 1.0 Angstrom, this approximation might be considered as acceptable. As a consequence, a single OT structure might be used as *representative* of the basin. For the sake of brevity, pictures and additional details about the representative OT structures for TT simulations are reported in the Supplementary Information. Here, it suffices to remark that only the region corresponding to basins I and L do actually correspond to structures somewhat similar to all-anti all-planar moieties. It follows that most stable conformations, i.e., most sampled TT geometrical states, show clear torsional excitations between vicinal thiophene rings as well as out-of-plane collective deviations of the whole polithiophene moiety.

The same analysis was then carried out for QT and DQT systems for which, as previously pointed out from the comment of Fig. 2, we may expect an almost identical conformational repertoire. As a matter of fact, the atomic components of the first two eigenvectors obtained from diagonalization of OT moiety covariance matrix from QT and DQT simulation, reported in Fig. 5a, b, show an almost perfect overlap. Moreover, see Fig. 5c, the projection of the QT and DQT trajectories in the plane constituted by the first two eigenvectors from QT covariance matrix also produces a very good overlap.

As a consequence of these observation, we have decided to carry out the extraction of the representative OT

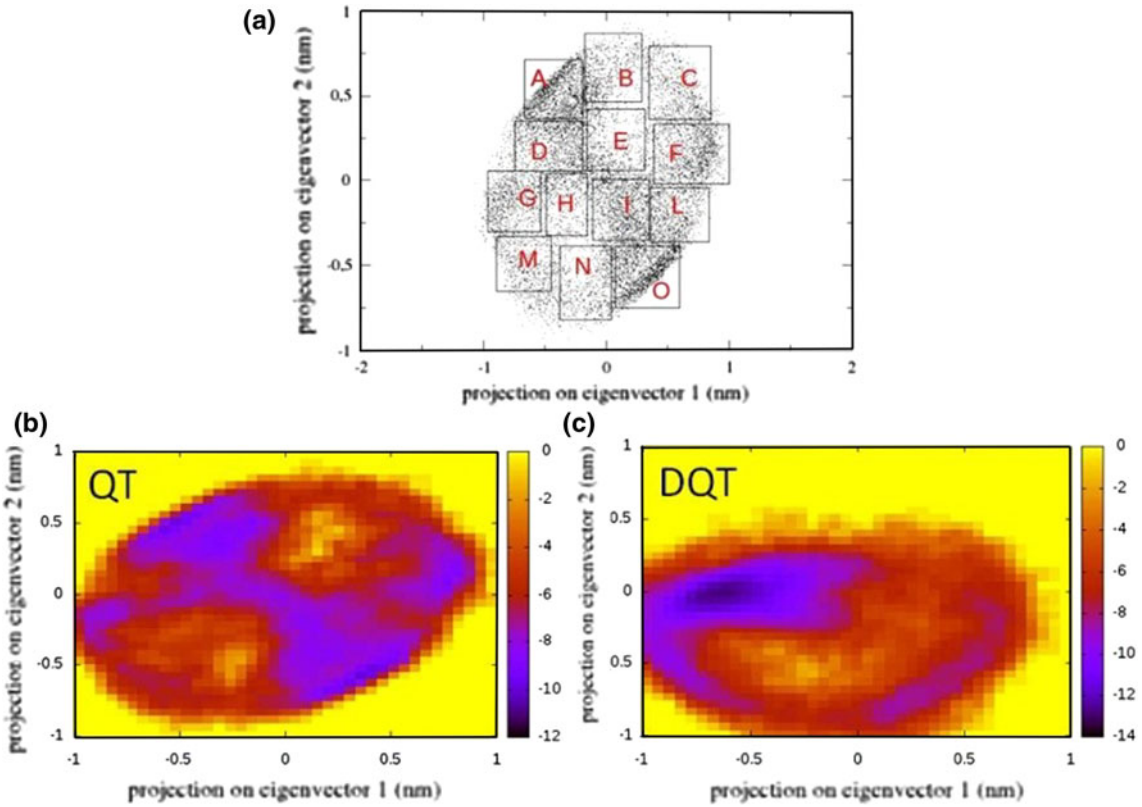

Fig. 6 **a** Identification of the conformational basins (*A–O*) in the OT essential plane from QT (DQT) MD simulation and **b** corresponding 300 K free energy landscapes (kJ/mol) for QT and DQT, from Eq. 7. Conformational basins are indicated with *red letters* and the representative structures are reported in the Supplementary Information. *Yellow* regions identify not sampled regions of the essential plane

structures for QT and DQT by using the same essential plane. The results presented below refer to the QT essential plane. Note, however, that the same procedure performed utilizing the DQT plane provided an almost identical result. The result is reported in the Fig. 6.

Similarly to TT, also for QT and DQT, many OT conformations—whose details are reported in the Supplementary Information—are populated a 300 K in solution with the *all-anti* all-planar structures (representative of basins A and O), representing the most stable ones. It is also interesting to note that the almost perfect symmetry emerged in the essential plane of TT and QT (unsubstituted species) is slightly but sharply broken in the case of DQT suggesting that the alkyl side chains do provide some differences also on the relative stabilities of OT conformations. The above analyses were finally repeated for the largest DET species.

The results, collected in Fig. 7, with the structural details also in this case reported in the Supplementary Information, indicate that also for DET, the *all-anti* structure (in this case falling in the basin A) is the most stable one with other conformations, however, significantly sampled during the trajectory. At this point, we are ready to utilize all the representative structures extracted for TT, QT, DQT, and DET for evaluating, by means of PMM-MD, the related spectra as described in the next two subparagraphs.

3.3 Calculation of UV spectra for TT, QT, DQT, and DET

Using the Schemes 1 and 2, within first-order approximation, i.e., Eq. 4, we evaluated the PMM-derived UV spectrum for each species. In particular, we analyzed the region between 300 and 600 nm. In Table 1, we schematically summarize the pre-selected QCs and the perturbing environment for each simulation.

Within the present model, in all the simulations, the solvent molecules produce an electrostatic (fluctuating) perturbation on the QCs. In the case of DQT and DET, beyond the solvent molecules, also the fluctuating alkyl side chains produce the perturbation.

Note that the actual spectra should arise from the convolution of the spectra of all the conformers with their own weight provided by the simulation ensemble as already reported in Scheme 2.

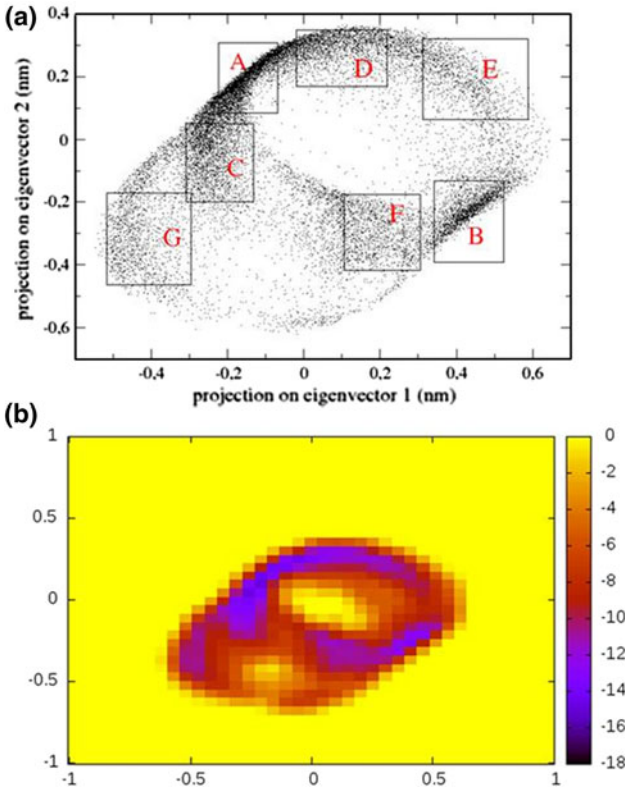

Fig. 7 **a** Identification of the conformational basins (*A*–*G*) in the OT essential plane from DET MD simulation and **b** corresponding 300 K free energy landscapes (kJ/mol) for DET from Eq. 7. Conformational basins are indicated with *red letters* and the representative structures are reported in the Supplementary Information. *Yellow* regions identify not sampled regions of the essential plane

By a practical point of view, Scheme 2 has been applied as follows.

Step 1 The QC conformations are extracted from their own basins (Sect. 3.2, Figs. 4, 6, 7 and Supplementary Information). We wish to point out that the size of each of these portions is arbitrary and its effect on the spectrum will be addressed later (see Step 5).

Step 2 According to Scheme 2 in correspondence of each structure representative of the different basins (Sect. 3.2, Figs. 4, 6, 7 and Supplementary Information), the unperturbed set of ground and eight excited states wavefunctions $\Phi_{l'}^{o-m}$ were obtained in vacuo (superscript 'o') using TD-DFT with B3LYP functional and 6–31 + G(d, p), with $l' = 0,1, 2,\ldots,8$ (note: 0 stands for ground electronic state) and $m = A, B, C,\ldots$. It is important to further remark that in the case of DQT and DET, the methyl groups were included in the unperturbed calculations in the 4–4‴ and 4–4⁗ positions, respectively.

Step 3 PMM is applied along the trajectory selecting the $\Phi_{l'}^{o-m}$ unperturbed set on the basis of the actual location on the essential plane evaluated by a root mean square deviation (RMSD)-based procedure (see Scheme 2) as reported in the Fig. 8.

More precisely: when the trajectory (blue line in Fig. 8) enters a selected area, e.g., basin H, the calculation of the RMSD carried with respect to all the structures will produce the minimal value in correspondence of the structure representative of basin H. Consequently, as far as this condition is hold along the trajectory, PMM is applied with the unperturbed basis for the QC structure H (i.e., $\Phi_{l'}^{o-H}$ with $l' = 0, 1, 2,\ldots,8$). As soon as the trajectory escapes from the basin H, the RMSD minimal value will turn out to fall in correspondence, let's say, of basin I whose unperturbed basis set (i.e., $\Phi_{l'}^{o-I}$ with $l' = 0, 1, 2,\ldots,8$) is then utilized for PMM.

Step 4 The spectrum of each species is evaluated following the Step 3 procedure, and the relative statistical weight of each species is automatically included.

Step 5 The choice of using a limited number of basins of an arbitrary area will obviously produce a non-continuous spectrum for which the calculation of *all* the points on the essential plane (all the conformations and not only the representative structures) would be required. In order to circumvent this practical drawback and whatever systematic deficiency arising from the arbitrariness of the size of the basin, we extracted four different structures in each of three different basins of TT simulation (namely: four structures in basin L, four in basin N and four in basin C). In each basin, we extracted the structures showing the largest root mean square deviation (which, however, as previously stated, does not exceed 1.0 Angstrom). On these structures, we calculated, in vacuum, the absorption frequency at the same level of theory then obtaining the corresponding standard deviation for each conformational basin. In this way, assuming no relevant variation for the standard deviation due to solvent effects and considering that for each basin, the corresponding dispersion was almost the same, we estimated the proper frequency standard deviation to be used for all the representative structures of the related basins as σ^2 equal to 3.1×10^{-6} a.u.^{2}. This value was then utilized to reconstruct the frequency fluctuation in each conformational basin via a Gaussian distribution centered at the basin mean frequency. This has been accomplished, in practice, by multiplying in each frequency bin, the spectrum value as obtained by steps 3 and 4 by such a Gaussian distribution and the bin size itself.

The S_0–S_1 spectra coming out from steps 1–4 are shown in Fig. 9 for TT, QT, and DQT. Note that in this case, the S_0–S_2 transition has been not included as producing a signal negligibly small.

Table 1 PMM system

SPECIES	QC	PERTURBATION
TT	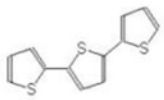	Solvent
QT	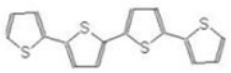	Solvent
DQT	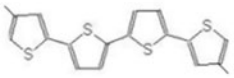	Solvent and 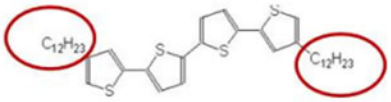
DET	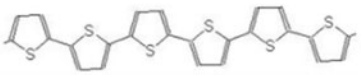	Solvent and 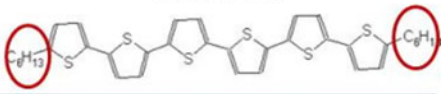

QC stands for the region explicitly treated at electronic level. Perturbation stands for the portion of the simulated system acting as an electrostatic perturbation on the QC. We wish to further remark that in the case of DQT and DET the substituent alky chains (i.e. $C_{12}H_{23}$ and C_6H_{13}) have been substituted in the unperturbed calculation with CH_3 groups in the same positions. Hence the perturbation is formally due to $C_{11}H_{20}$ and C_5H_{10}, respectively

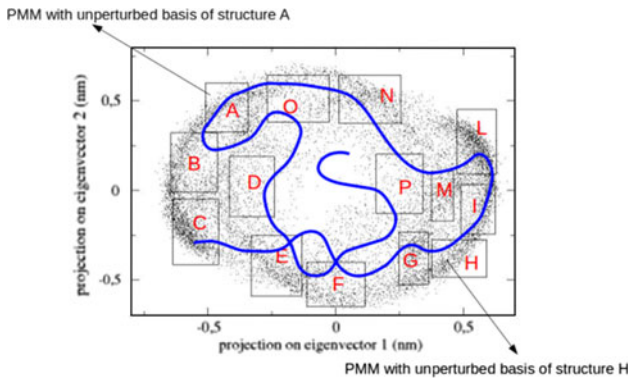

Fig. 8 Schematic representation of the time evolution of the trajectory onto the essential plane

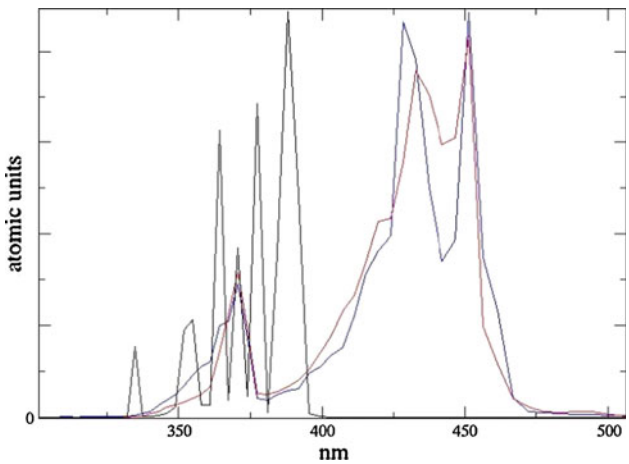

Fig. 9 Superposition of S_0–S_1 transitions (spectrum) resulting from steps 1–4 for TT (*black*), QT (*blue*), and DQT (*red*)

The spectra resulting from the steps 1–5 are then reported in the Fig. 10a–c for TT, QT, and DQT for the first and second electronic transition.

Note also that S_0–S_2 have been reported only for TT and QT as we did not appreciate any difference for this signal in the case of QT and DQT.

In Fig. 11, we have finally reported the spectrum for DET, compared with the one of QT.

As already remarked in the Theoretical section, the use of the first-order approximation in the construction of the electronic perturbed Hamiltonian (Eq. 4), utilized for the spectra previously shown, may produce artifacts and unrealistic electrostatic QC-environment interactions in particular when long-shaped QCs are concerned. For this reason, we have evaluated the spectral features also using the second-order approximation (Eqs. 1–3). This has been carried out for all the systems and shown for the largest one, i.e., DET.

The result, reported in Fig. 12, shows that in the case of DET, the presence and the absence of the second-order

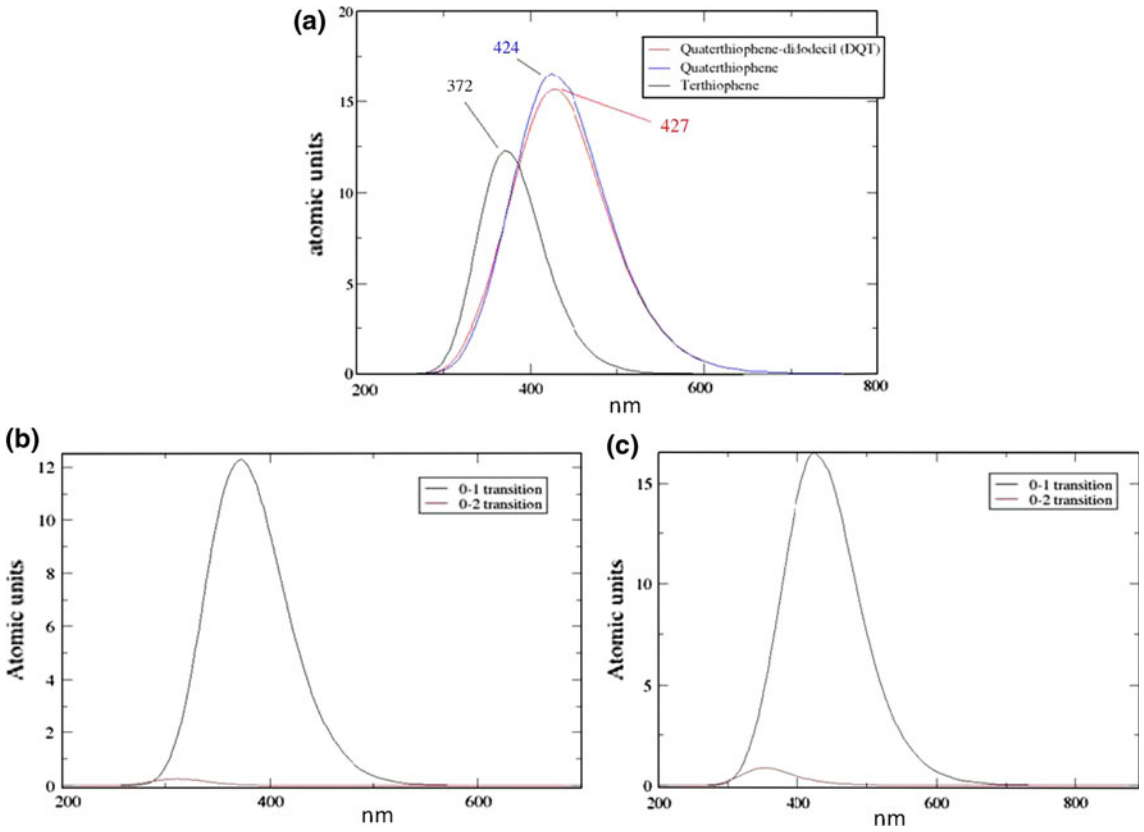

Fig. 10 **a** Comparison of 0–1 transition for TT, DQT, and QT. **b** Comparison of S_0–S_1 and S_0–S_2 transition for TT. **c** Comparison of S_0–S_1 and S_0–S_2 transition for QT

term in the operator do not appreciably alter the result. The strong similarity between all the reported points, probably due to the relatively large value of the ground-state dipole confining within the noise the effect of the quadrupole-electric field gradient interaction, clearly suggests that the description up to the dipolar interaction is sufficient in this case in the species addressed in this work.

4 Discussion

The previously described computational and experimental results have been summarized in the following Table 2.

As already remarked in the Introduction, the above data do not include two important aspects: the basis set for Perturbed Hamiltonian is not based on multi-reference calculations and the vibronic effects are not included. It is interesting to observe that despite the above limitations, the experimental sequence for S_0–S_1 transition, i.e., from TT to DET, as well as the experimental bandshapes are both rather well reproduced. The only severe discrepancy arising from the comparison between calculated and experimental spectra is the systematic under-estimated od the simulated spectral maxima. This effect, having already excluded systematic deficiencies of the first-order definition of the Hamiltonian operator (Fig. 12), might be principally ascribed to the already cited limitations of TD-DFT unperturbed calculations. It follows that other important plausible source of error, i.e., the lack of vibronic coupling, seems not to dramatically alter in this case the final picture. This might be partially ascribed to the fact that the large spectral broadening induced by conformational transitions of the chromophore in solution, i.e., by excitation of classical internal degrees of freedom and inhomogeneous interaction with solvent electric field, almost completely overwhelms the vibronic fine structure. This is obviously a supposition which deserves more accurate deep investigation. Hence, well aware of the previously remarked intrinsic limitations of the computational setup, let us illustrate some key points emerging from our results.

First of all, we wish to remark the presence of the S_0–S_2 signal red shifted with respect the S_0–S_1 one. This result, very difficult to be proved in solution, nicely fits early experimental observations carried out for OT with 2 up to 5 monomers [5].

The most interesting aspect emerging from our study resides in the importance of the inclusion of different conformations in the evaluation of the spectral UV

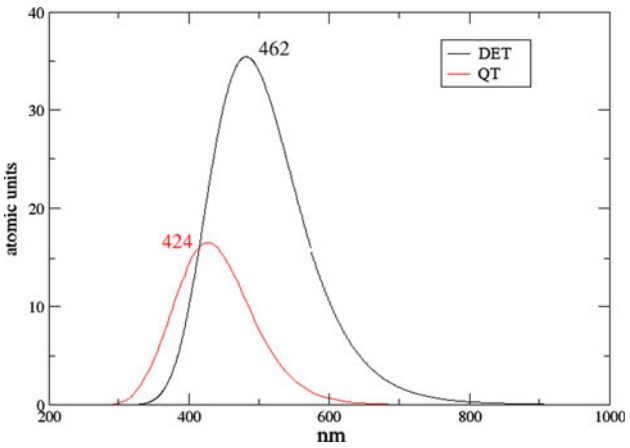

Fig. 11 Comparison of S_0–S_1 transition for DET and QT

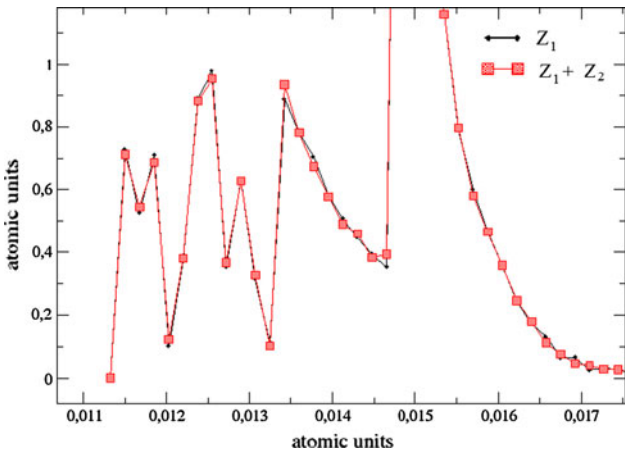

Fig. 12 Comparison between DET spectrum (without application of step 5) within first order, Z_1 (*black diamonds*, Eq. 4) and second order, $Z_1 + Z_2$ (*red squares*, Eq. 1) definition of the perturbed Hamiltonian operator. Note that the linear (energy) scale has been used in this case and not the wavelength

transition in solution which can be shortly summarized in Fig. 13 where we have reported, for each species (free energy basin) the excitation energies experienced during the simulation and the excitation energy in vacuum.

The above findings clearly indicate that:

- we do not observe any red spot (i.e., the value of 0–1 transition in vacuum) outside the black regions (the distribution of the 0–1 transitions perturbed along MD simulation).
- the black regions span a rather large energy range, in some cases (i.e., for some OT conformations) *very* large (more than 100 nm).
- The red spots may vary even in a relevant fashion when passing from one conformer to the other one.

This implies that:

- the maximum of the absorbance (roughly speaking the average absorption wavelength) is not dramatically influenced by the solvent (or more in general by the electrostatic perturbation).
- the solvent (or more in general the electrostatic perturbation) does have a strong effect on the *shape* of the spectrum resulting in sharp enlargements of the absorbing range even on a single conformation immersed in the fluctuating solvent.
- Different conformations of the same molecule may not only result in a different (sometimes *very* different) ground- to excited-state energy (shift of the red spots) but also in a very different *response* to the electrostatic perturbation (black spots distributed over long 'chains').

As a consequence of these finding, it turns out that when one has to model the OT electronic properties in condensed state and in thermal conditions, i.e., the typical OT working conditions, it is important to carefully consider all the conformations sampled in solution and also their interaction with the solvent. As a matter of fact, different OT conformations in interaction with the solvent do actually represent molecular systems with very different photophysical properties and, at least in principle, an external action leading to the alteration of the OT conformational equilibrium may produce dramatic alterations of the overall electronic properties.

In order to provide further insights into the OT photophysics and how it is influenced by thermal and environmental effects, we have more carefully investigated the changes in the charge distribution upon OT excitation. This has been accomplished by evaluating the *perturbed* electric dipole (Eq. 6) of the OT first excited electronic state, $\boldsymbol{\mu}_{\text{first excited}}$ and its projection the *perturbed* electric dipole of OT ground state, $\boldsymbol{\mu}_{\text{ground}}$. We indicate such a projection as $\boldsymbol{\mu}_{\text{ground}} \cdot \boldsymbol{\mu}_{\text{firstexcited}}$ It is first important to remark that $\boldsymbol{\mu}_{\text{ground}}$ undergoes a scarce fluctuation in solution. As a matter of fact (see Supplementary Information), its projection along the simulation onto the unperturbed ground-state dipole produce a value essentially always equal to one. Hence, a value of $\boldsymbol{\mu}_{\text{ground}} \cdot \boldsymbol{\mu}_{\text{firstexcited}}$ very different to 1 would imply an intra-molecular (intra OT moiety) charge transfer, i.e., a substantial reorganization of the perturbed electronic distribution upon excitation.

The resulting picture is reported in Fig. 14 where we have correlated $\boldsymbol{\mu}_{\text{ground}} \cdot \boldsymbol{\mu}_{\text{firstexcited}}$ values with the corresponding excitation energy along the overall trajectory.

In this Figure, a projection equal to one for a given excitation wavelength implies that upon such a ground- to first-excited-state vertical excitation, the OT first-excited-state

Table 2 Comparison of the calculated and experimental absorption maxima

Species	Calculated S_0–S_1 absorbance maximum (nm) ($\Delta\lambda$ with respect to TT)	Experimental S_0–S_1 absorbance maximum (nm) ($\Delta\lambda$ with respect to TT)	Calculated S_0–S_1 half maximum width (nm)	Experimental S_0–S_1 half maximum width (nm)
TT	372 ± 2 (0)	355 (0)	90	80
DQT	427 ± 2 (+55)	398 (+43)	110	100
QT	424 ± 2 (+52)	393 (+38)	120	100
DET	462 ± 2 (+90)	415 (+60)	100	100

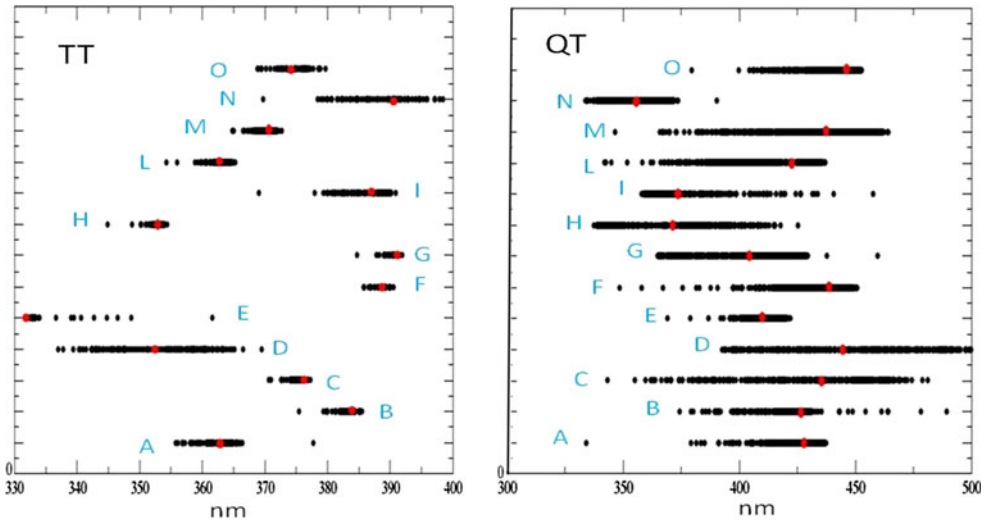

Fig. 13 Gas-phase (*red spots*) and solvent-perturbed (*black spots*) S_0–S_1 transition wavelengths along TT and QT simulations for each free energy basin (representative conformations). Note that basin P (Fig. 5) for TT has not been reported as scarcely sampled

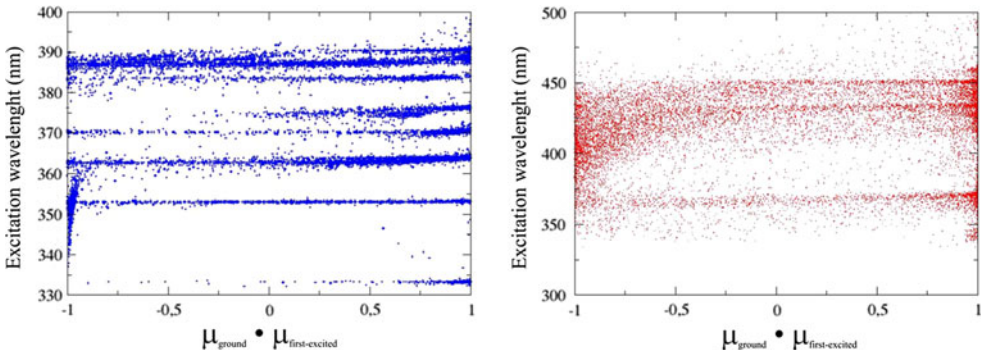

Fig. 14 Correlation between electronic energy excitation and charge fluctuation in the first excited state of TT (*left panel*) and QT (*right panel*). Value of the abscissa equal to 1

dipole moment—i.e., OT first-excited-state electronic density—does not undergo appreciable variation. Consequently, all the other values of the projection indicate intramolecular charge fluctuation upon the specific excitation. Our result shows that when OT vertically accesses the S_1 electronic state the occurrence of intra-molecular charge transfer strongly depends both on the instantaneous field exerted by the solvent on the QC and on the QC geometry itself. As a matter of fact, at a given value of excitation wavelength, the electronic response of OT moiety ($\boldsymbol{\mu}_{\text{ground}} \cdot \boldsymbol{\mu}_{\text{firstexcited}}$) does span the whole domain from −1 to 1. However, e.g., in the case of TT depicted in the left-side panel of Fig. 14, it is possible to extract narrow photon energies between 340 and 350 nm and between 355 and 360 nm corresponding to $\boldsymbol{\mu}_{\text{ground}} \cdot \boldsymbol{\mu}_{\text{firstexcited}}$ values equal to −1, i.e., indicating an intramolecular charge transfer.

Such a result, somewhat speculative, might provide a good starting point for modeling the possibility of designing perturbing field for controlling the possibility of intramolecular electron transfer in complex environments [50].

5 Conclusions

The S_0–S_1 and S_0–S_2 electronic excitations for a series of polycyclic thiophene oligomers (OT), extensively used in organic electronics and solar cells, have been studied

experimentally and theoretically in dilute dichloromethane solution. It emerges that the electronic properties of the OT low-lying excited states might result very different when different conformations, even energetically very close, are sampled in solution at 300 K. This finding confirms that the thermal and environmental effects, beyond an advanced description of the electronic excited states and the inclusion of the vibronic effects, are very important for better understanding the photophysics of these systems in liquid solutions. Further aspects, essentially related to the characterization of OT low-lying excited states in solution, also indicate that a subtle combination of solvent electric field and OT conformational transition might induce intramolecular electron transfer and virtually open the possibility of designing a proper OT-environment condition for controlling electron transfer processes.

References

1. Horowitz G, Garnier F, Yassar A, Hajlaoui R, Kouki F (1996) Adv Mater 8:52
2. Pal AJ, Ostergard T, Paloeimo J, Stubb H (1997) Phys Rev B Condens Matter 55:1306–1309
3. Alem S, Pandey AK, Unni KNN, Nuzi JM, Blanchard P (2006) J Vac Sci Technol A 24:645–648
4. Taliani C, Gebauer W (1999) In: Fichou D (ed) Handbook of oligo and polythiophenes. Wiley, Weinheim
5. Becker RS, Seixas de Melo J, Macanita AL, Elisei F (1995) Pure & Appl Chem 67:9–16
6. Salzner U (2007) J Chem Theory Comput 3:1143–1157
7. Fabiano E, Della Sala F, Cingolani R, Weimer M, Gurling A (2005) J Phys Chem A 109:3078–3085
8. Siegert S, Vogelert F, Marian CM, Weinkauf R (2011) Phys Chem Chem Phys 13:10350–10363
9. Beljonne D, Cornil J, Friend RH, Janssen RAJ, Bredas L (1996) J Am Chem Soc 118:6453–6461
10. Giershner J, Mack HG, Egelhaaf HJ, Schweizer S, Doser B, Oelkrug D (2003) Synth Met 138:311–315
11. Garcia M, Guadarrama P, Fomine S (2010) J Phys Chem A 114:5406–5413
12. Fujitsuka M, Nakatani T, Sakamoto M, Sugimoto A, Majima T (2010) J Phys Chem A 114:10789–10794
13. Colditz R, Grebner D, Helbig M, Rentsch S (1995) J Phys Chem 201:309–320
14. Telesca R, Bolink H, Yunoki S, Hadziioannou G, Th. Van Duijen P, Snijders JG, Jonkman HT, Sawatzky GA (2011) Phys Rev B Condens Matter 63:155112
15. Della Sala F, Heinze HH, Gorling A (2001) Chem Phys Lett 339:343–350
16. Rubio M, Merchan M, Pou-Amerigo R, Orti E (2003) ChemPhysChem 4:1308–1315
17. Rubio M, Merchan M, Orti E (2005) ChemPhysChem 6:1357–1368
18. Risko C, McGehee MD, Bredas JL (2011) Chem Sci 2:1200–1218
19. Macchi G, Miliàn Medina M, Zambianchi M, Tubino R, Cornil J, Barbarella G, Giershner J, Meinardi F (2009) Phys Chem Chem Phys 11:984–990
20. Milian Medina B, Wassenberg D, Meskers SCJ, Janssen RAJ, Mena-Osterit E, Bauerle P, Grierchner J (2008) J Phys Chem A 112:13282–13286
21. Gierschner J, Cornil J, Egelhaaf HJ (2007) Adv Mater 19:173–191
22. Aleman C, Julià L (1996) J Phys Chem 100:1524
23. Aleman C, Julià L (1996) J Phys Chem 100:14661
24. Roncali J (1992) Chem Rev 92:711
25. Barbarella G, Bongini G, Zambianchi M (1994) Macromolecules 27:3039
26. Egelhaaf HJ, Gierschner J, Oelkrug D (2002) Synth Met 127: 221–227
27. Barbarella G, Bongini G, Zambianchi M, Antolini L (1992) Adv Mater 4:282
28. Amadei A, D'Alessandro M, D'Abramo M, Aschi M (2009) J Chem Phys 130(8):08410
29. Amadei A, D'Abramo M, Zazza C, Aschi M (2003) Chem Phys Lett 381:187
30. Zazza C, Amadei A, Sanna N, Grandi A, Chillemi G, Di Nola A, D'Abramo M, Aschi M (2006) Phys Chem Chem Phys 8:1385
31. Aschi M, Fontana A, Di Meo E, Zazza C, Amadei A (2010) J Phys Chem B 114(5):1915–1924
32. Improta R, Barone V (2004) J Am Chem Soc 126:14320–14321
33. Marini A, Munoz-Losa A, Biancardi A, Mennucci B (2010) J Phys Chem B 114:17128–17135
34. Amadei A, Marinelli F, D'Abramo M, D'Alessandro M, Anselmi M, Di Nola A, Aschi M (2005) J Chem Phys 122:124506
35. Parac M, Grimme S (2003) Chem Phys 292:11
36. Gross EKU, Dobson JF, Petersilka M (1996) In: Nalewajski RF (ed) Density functional theory II, Springer series in topics in current chemistry, band 181. Springer, Heidelberg
37. Gao J (1996) Rev Comp Chem 7:119–185
38. Moreno M, Casalegno M, Raos G, Meille SV, Po' R (2010) J Phys Chem B 114(4):1591–1602
39. Duffy EM, Severance DL, Jorgensen WL (1992) J Am Chem Soc 114:7535–7542
40. Amadei A, Chillemi G, Ceruso MA, Grottesi A, Di Nola A (2000) J Chem Phys 112:9–23
41. Berendsen HJC, Postma JPM, van Gunsteren WF, Di Nola A (1984) J Chem Phys 81:3684–3690
42. Hess B, Bekker H, Berendsen HJC, Fraaije JGEM (1997) J Comput Chem 18:1463–1472
43. Darden TA, York DM, Pedersen LG (1993) J Chem Phys 98:10089
44. Van der Spoel D, van Buren AR, Apol E, Meulenhoff PJ, Tieleman DP, Sijbers ALTM, van Drunen R, Berendsen HJC (1996) Gromacs user manual version 1.3
45. Amadei A, Linssen ABM, Berendsen HJC (1993) Proteins Struct Funct Genet 17:412–425
46. Becke AD (1993) J Chem Phys 98(2):1372–1377
47. Lee C, Yang W, Parr RG (1998) Phys Rev B 37(2):785–789
48. GAUSSIAN Frish MJ et al (2004) Gaussian 03, Revision C.02 Gaussian Inc. Wallingford, CT
49. Yang L, Feng JK, Ren AM, Sun JZ (2006) Polymer 47:1397–1404
50. Zhao J (2002) Chem Phys Lett 351:481–485